Numerical Investigation of Granular Flow in a Shear Cell

X. Wang[1], H.P. Zhu[2], A.B. Yu[1] and S. Luding[3]

[1]School of Materials Science and Engineering, The University of New South Wales, Sydney, NSW 2052, Australia
[2]School of Computing, Engineering and Mathematics, University of Western Sydney, Locked Bag 1797, Penrith, NSW 2751, Australia
[3]Multi Scale Mechanics, CTW, MESA+, University of Twente, PO Box 217, 7500 AE Enschede, Netherlands

Abstract. Granular flow in a shear cell under conditions relevant to those in an annular cell is investigated based on the results obtained by using the Discrete Element Method. The distributions of porosity and coordination number are studied, and the relationship of these variables is established. The so-called *I*-rheology proposed by Jop et al. [Nature (London) 441, 727 (2006)] is tested. The results display that the *I*-rheology can effectively describe the intermediate flow regime, whereas significant deviations take place when it is applied to the quasi-static regime. The correlations between stresses and packing fraction are examined and the packing fraction values for the quasi-static/intermediate and intermediate/inertial regime transitions are identified. The force networks/structures for different scaled stiffness are analyzed to further understand the regime-transitions for the granular flow.

Keywords: Discrete element method, shear cell, granular dynamics, flow regimes, structural analysis
PACS: 45.70.Mg, 45.70.Vn, 47.57.Gc

INTRODUCTION

Shear testers are classical devices, widely used to measure the flow properties of particulate materials such as the macroscopic angle of friction and the relationship between shear and normal stresses [1]. One of the typical shear testers is the annular shear cell. Previous studies on such annular shear cells are mainly based on experimental approaches, and focused on attrition behavior [2], external stress profile and transport property measurements [3]. The main issue with such experimental approaches is that they can only offer a relatively global, bulk scale picture of the particle flow in an annular shear cell and cannot provide much of microscopic or particle scale information, which is useful to better understand the working principles of particulate flow in annular shear cells. While it is difficult to obtain complete particle-scale information by means of physical experiments at present, computer simulations offer a convenient and cost-effective alternative way [4,5].

In the present work, the discrete element method (DEM) is employed to produce particle scale information of granular flows, which can offer insights into the operation of annular shear cells. The resulting information is analyzed in terms of the spatial distributions of microscopic and macroscopic variables and their inter-relationships. The results are useful to further understand the fundamentals underpinning the application of annular shear cells.

SIMULATION CONDITIONS

In the annular shear cell considered here, particles are bounded by a stationary upper, and a moving lower plate with stationary inner and outer cylindrical walls. To improve computational efficiency, only a flat, rectangular segment of the shear cell is simulated (Fig. 1) and periodic boundary conditions are used to mimick the cylindric-symmetrical geometry of the whole annular space. The cells bottom and top plates are perpendicular to the *Z*-axis, two stationary walls are perpendicular to the *Y*-axis, and two periodic boundary planes are perpendicular to the *X*-axis. Both the upper and lower plates of the cell are roughened by 360 spherical particles, with diameter d, and no relative movement. The sheared material in the cell consists of 5000 spherical particles with the same diameter d. The cell dimensions are $12d$ and $30d$ in *X*- and *Y*-directions, respectively, while the height (*Z*) is varying due to normal stress and shear velocity. The material properties used are: Young's modulus: 2.5×10^6 $\pi\rho dg/6$, Poisson's ratio 0.3, sliding friction coefficient 0.5, and rolling friction coefficient $0.01d$. The effects of normal pressure and shear velocity are considered. The base values for the two variables are

Powders and Grains 2013
AIP Conf. Proc. 1542, 531-534 (2013); doi: 10.1063/1.4811985

1947.8 πρdg/6, and 6.2 √gd, respectively. The units of shear velocities are √gd in this paper.

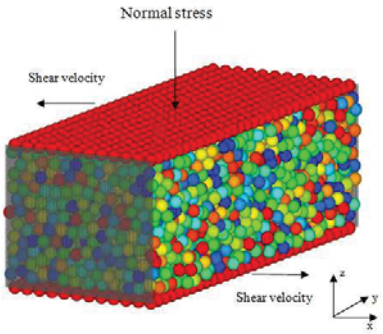

FIGURE 1. Section selected for simulating the shear cell under applied normal stress and shear velocities on the top- and bottom-plates.

RESULTS AND DISCUSSION

The movement of particles in the regions close to the plates is mainly driven by the interaction forces between particles and the plates. As a result, the particles in those regions have large velocity, directed in the same direction as the corresponding plate. For the regions far from the plates, the dissipative frictional interaction prevails, preventing particles from sliding relative to each other. The resulting velocities decrease away from the walls, in the two flow directions, and counterbalance each other in the middle, resulting in a negligible flow velocity there.

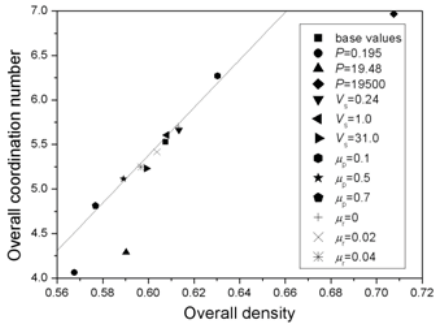

FIGURE 2. Correlation between overall coordination number, C_n, and packing density for different cases (the solid line is from the correlation C_n =26.8ν-10.7).

Porosity and coordination number are the two parameters commonly used to describe the isotropic local structure in a particle system. Our simulations show that porosity is high in the regions near the plates and low in the middle part of the cell. In the majority of the cell space, the coordination number is distributed in a narrow range of 5 to 5.8 with a rather symmetrical pattern. A linear relationship between overall coordination number and packing density is shown in Fig. 2, where most points collapse on a master curve C_n=26.8ν-10.7. Strong deviations to the relation take place in three cases, all of which correspond to different normal pressure, which might be due to a structural transition of the system in response to the change of the normal pressure.

One of the basic applications of an annular shear cell is the establishment of a relationship between shear and normal stresses, which is essential in examining the particle flow properties. In order to explore this relationship, the values of shear and normal stresses are plotted in Fig. 3. It should be noted that the particles/contacts in the regions close to the walls are excluded, since the dynamic behavior is much more complex in these regions due to the effect of couple-stress. The data are slightly scattered for all the four shear velocities. Despite scatter, a linear trend between the internal shear and normal stresses can be seen for all four shear velocities. The values of the corresponding friction coefficients are approximately 0.349, 0.351, 0.360 and 0.369, for the four shear velocities 0.24, 1.0, 6.2 and 31.0, respectively.

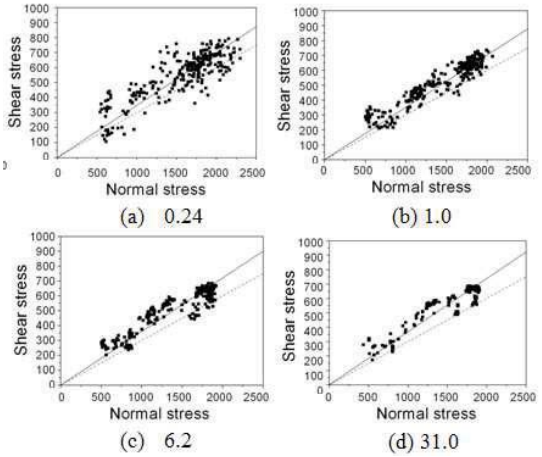

FIGURE 3. Relationship between internal shear and normal stresses for different shear velocities, as given above. The dashed line in each figure has a slope of 0.3, corresponding to the inter-particle friction coefficient used in the DEM code. The solid line in each figure gives the best fit for the corresponding data set.

Furthermore, we have considered the dependence of the internal friction coefficient (μ) on the inertial number (I) at the four different shear velocities, as shown in Fig. 4. For the shear velocities of 0.24 and 1.0, the data are very scattered, indicating that the correlation between inertial number and internal friction coefficient is poor for these slowly sheared systems. Conversely, the dependence of the internal friction coefficient on I is relatively clear for the shear velocities of 6.2 and 31.0, in spite of several deviating

points. We try to fit the present results with the *I*-rheology: $\mu(I) = \mu_1 + (\mu_2 - \mu_1)/(I_0/I + 1))$, as proposed by Jop et al. [6], and found that the form can fit the data corresponding to the shear velocity of 6.2 or 31.0 well with a high correlation coefficient of 0.85, as shown in the inset of Fig. 4. However, the fit of the form to the data corresponding to the shear velocity of 0.24 or 1.0 is very poor. The deviation may be due to intermittent velocity fluctuations or non-local effects resulting from the fluctuations in the quasi-static regime, as indicated in previous studies [7,8].

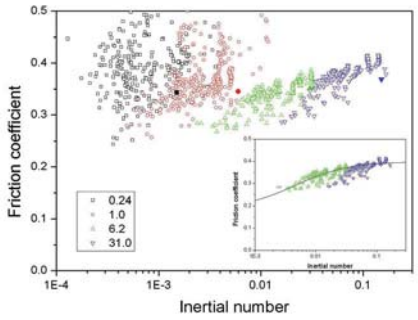

FIGURE 4. Dependence of the internal friction coefficient on the inertial number for four different shear velocities. The solid line in the inset is the best fit for the shear velocities of 6.2 and 31.0 combined with parameters (μ_1, μ_2, I_0) = (0.186, 0.398, 0.00466) in $\mu(I)$, as proposed by Jop et al. [6].

To determine the transition between flow phases in the cell, we consider the elastically scaled stress, $\sigma^*=\sigma d/k$, the kinetically scaled stress, $\sigma'=\sigma/\rho d^2 \dot{\gamma}^2$, and the scaled stiffness, $k^*=k/\rho d^3 \dot{\gamma}^2$, where σ is the applied normal stress, ρ is the materials mass-density, d is the particle diameter, $\dot{\gamma}$ is the effective (local) shear rate due to the plates and k is the material contact stiffness. Figure 5(a) shows the dependence of the elastically scaled applied stress on packing fraction (ν) for different values of the scaled stiffness. When $\nu \geq 0.58$, the data corresponding to different values of k^* tend to collapse onto one master curve, indicating that the elastically scaled stress of the dense systems is independent of k^* (and thus the shear rate) in the quasi-static regime. For $\nu < 0.58$, the data for different k^* start to deviate from each other, implying the appearance of inertial effects. As a result, $\nu = 0.58$ is a critical value that separates the quasi-static from the intermediate regime. Figure 5(b) shows the correlation between kinetically scaled stress and packing fraction. When the packing fraction is high (e.g. $\nu \geq 0.58$), the data of σ' for different values of k^* display significant differences, showing that the kinetically scaled stress is greatly dependent on k^* for shear rates in the quasi-static regime. As the packing fraction decreases, the difference becomes smaller. In particular, the data collapse into one master curve for ν below 0.5. The fact that the data can fall onto one master-curve indicates that the stress for all the flows scales kinetically with packing fraction and thus the flows are in the inertial regime.

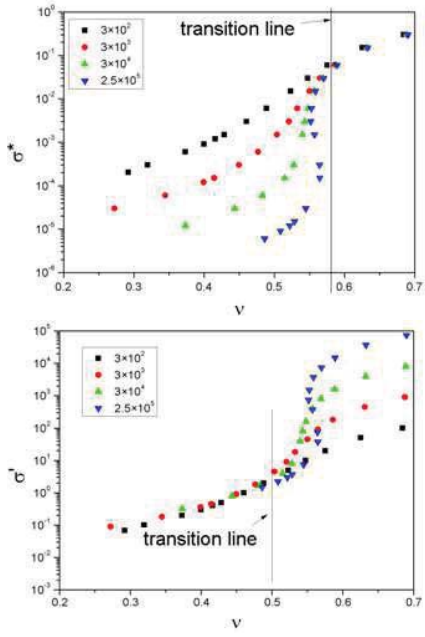

FIGURE 5. Variations of (a) elastically scaled applied stress (σ*) and (b) kinetically scaled applied stress (σ'), with packing fraction (ν) for different values of scaled stiffness, as given in the inset.

With the transition point known, see the above discussion, we are able to condense the flow regime maps in the range of the parameters used in this work, as shown in Fig. 6. On one hand, if k^* (and shear rate) is fixed, a decrease in σ* causes the system to change from the quasi-static regime, through transients, to the inertial regime. This is a reasonable outcome because

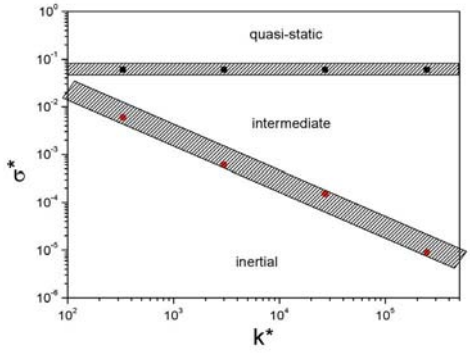

FIGURE 6. Regime map in the parametric space of (σ*, k*).

for a given shear rate, decreasing the applied stress reduces the constraint on the system, which makes the system expand (dilate). The need for particles to form force chains to counterbalance the normal loading is reduced. On the other hand, when σ* (applied stress) is fixed and very large, the system always stays in the quasi-static regime no matter what value the shear rate is (within the examined range), i.e. there is no access path between quasi-static and intermediate regimes in the parametric space of (σ*, *k**).

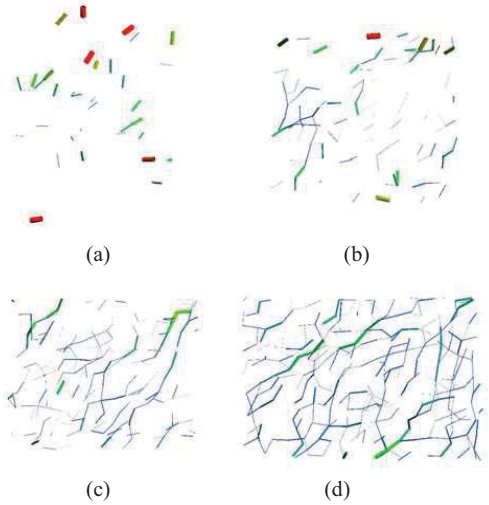

FIGURE 7. Networks of large scaled forces (f >1, where f is defined as the ratio of a normal contact force to the average normal contact force) for k*=3×102 for different values of σ*: (a) 3×10^{-4}; (b) 3×10^{-3}; (c) 1.5×10^{-2}; (d) 0.15.

In order to qualitatively examine the local, microscopic structure in this shear flow situations, we examine the contact networks under different conditions. Both Figs. 7(a) and 7(b) depict the profile of large scaled forces in the inertial regime. The difference is that the case in Fig. 7(b) is closer to the boundary between inertial and intermediate regimes. The main interaction mode in Fig. 7(a) is binary collisions, with no force chains formed in the system. This clearly corresponds to the traditional rapid flow or the inertial-collisional regime reported in [9,10]. In Fig. 7(b), some local particle clusters appear, implying that the flow could be deep into the so-called inertial-non-collisional regime [9,10], which may include not only particle clusters but also short force chains for some cases. In Fig. 7(c), system-spanning force chains start to form in the intermediate regime with increasing connectivity. Considering that the force chains are very short in the inertial flow regime, we may conclude that the appearance of system-spanning force chains can be used as an indication of the appearance of quasi-static effects. As σ* increases further, the number of the system-spanning force chains grows and the inertial effect (i.e. no force chains) is gradually 'squeezed' out of the system. When the inertial effect disappears with the application of higher normal stresses, the system enters the quasi-static regime, as shown in Fig. 7(d), with a dense force-network.

CONCLUSIONS

In the present study, the shearing of particles in a model shear cell has been investigated numerically using the DEM. There is a linear relationship between the overall coordination number and the packing density, for coordination numbers between 5 and 6.5. The relationship between the internal (contact) friction coefficient and the inertial number is fitted well with the *I*-rheology model proposed by Jop et al. [6] for the two cases of intermediate flow. However, large scattering exists in the relationship for the quasi-static flows. The packing fraction (v) can be used to identify the quasi-static/intermediate and intermediate/inertial regime transitions. The data collapse between σ* and v for different k* for v>0.58 is considered as an indication of the quasi-static regime, while the data collapse between σ' and v for different k* for v<0.5 is deemed as an indication of the inertial regime. The analysis of the force structures further helps to understand the microscopic origins for the macroscopic phase/regime transition in granular flows. An extension of the *I*-rheology involving also the tensorial nature of strain, stress, and structure will shed further light onto the interesting behavior of powders and grains [11].

REFERENCES

1. J. Schwedes, *Granular Matter* **5**, 1-43 (2003).
2. A.U. Neil and J. Bridgwater, *Powder Technol.* **80**, 207-219 (1994).
3. S.S. Hsiau, and W.L. Yang, *Phys Fluids* **14**, 612–621 (2002).
4. H.P. Zhu, Z.Y. Zhou, R.Y. Yang and A.B. Yu, *Chem. Eng. Sci*. **63**, 5728-5770 (2008).
5. H.P. Zhu, Z.Y. Zhou, R.Y. Yang and A.B. Yu, *Chem. Eng. Sci*. **62**, 3378-3396 (2007).
6. P. Jop, Y. Forterre and O. Pouliquen, *Nature* **441**, 727-739 (2006).
7. J. Gaume, G. Chambon and M. Naaim, *Phys. Rev. E* **84**, 051304 (2011).
8. D.L. Hennan and K. Kamrin, *PNAS* **110**(17), 6730-6735 (2013).
9. C.S. Campbell, *J. Fluid Mech*. **465**, 261-291 (2002).
10. C.S. Campbell, *J. Fluid Mech*. **539**, 273-297 (2005).
11. T. Weinhart, R. Hartkamp, A.R. Thornton, and S. Luding, *Phys. Fluids* in press (2013).